J. Biochem. 2009;145(4)543–554
doi:10.1093/jb/mvp009

Interactions Between Histidine and Tryptophan Residues in the BM2 Proton Channel from Influenza B Virus

Kohei Otomo, Akira Toyama*, Takashi Miura and Hideo Takeuchi†
Graduate School of Pharmaceutical Sciences, Tohoku University, Aobayama, Sendai 980-8578, Japan

Received December 16, 2008; accepted January 10, 2009; published online January 20, 2009

The BM2 protein of influenza B virus forms a transmembrane proton channel essential for the virus infection. We investigated the structure and mechanism of the BM2 proton channel by using a 31-mer peptide (BM2-TMP) representing the putative transmembrane domain of BM2, with special focus on His19, Trp23 and His27. Like the full-length protein, BM2-TMP formed a transmembrane proton channel activated at acidic pH with a midpoint of transition at pH 6.4 ± 0.1. Mutation of His19 to Ala almost abolished the channel activity, whereas the His27-to-Ala mutant retained partial activity. The proton selectivity of the channel was lost upon substitution of Phe for Trp23. Comparison of CD, fluorescence and Raman spectra measured for wild-type and mutated BM2-TMP at varied pH showed the pK_a of the imidazole ring to be ~6.5 for His19 and ~7.6 for His27. Analysis of the pH-dependent fluorescence and Raman intensities suggested the occurrence of cation−π interaction between the protonated imidazole ring of His and the indole ring of Trp. The His19−Trp23 cation−π interaction below pH 6.5 is likely to trigger the opening of the proton channel, whereas His27 is not essential but enhances the channel activity through interaction with Trp23, which constitutes the proton-selective gate.

Key words: cation-π interaction, histidine, influenza virus, proton channel, tryptophan.

Abbreviations: A/M2, M2 protein of influenza A virus; BM2-TMP, 31-mer peptide representing the putative transmembrane domain of BM2; DPX, *p*-xylene-bis-pyridinium bromide; M2-TMP, 25-mer peptide representing the putative transmembrane domain of A/M2; POPE, 1-palmitoyl-2-oleoyl-*sn*-glycero-3-phosphoethanolamine; POPS, 1-palmitoyl-2-oleoyl-*sn*-glycero-3-[phospho-L-Serine].

Replication of influenza virus critically depends on the proton channel activity of a protein encoded by the virus itself (*1*, *2*). The M2 protein of influenza A virus (A/M2) is one of such proteins and the proton channel formed by A/M2 in the virion envelope is activated at acidic pH (*3–5*). After penetration of the virion into the host cell through receptor-mediated endocytosis, the A/M2 channel opens to allow proton influx from the acidic endosomal compartment into the virion. The resultant acidification of the virion interior induces disassembly of the proteins lining the inner leaflet of the virus envelope, leading to virus uncoating and release of the viral genome into the host cell (*6*, *7*). An additional involvement of the A/M2 channel is also proposed in the transport process of an acid-sensitive viral protein to the host cell surface for assembly of progeny virions (*8*, *9*).

The A/M2 proton channel is a homotetramer of a 97-residue transmembrane protein (*10*, *11*), and its structure and mechanism have been studied extensively. A 25-residue peptide (M2-TMP, Fig. 1) representing the putative transmembrane domain of A/M2 has been found to form a proton channel analogous to that of the full-length protein (*12*, *13*). The channel consists of a bundle of four helices tilted from the membrane normal (*12*, *14–19*). Of the amino acid residues on the transmembrane helix, His at position 37 (His37) and Trp at position 41 (Trp41), which are one helix pitch apart from each other, are essential for the proton-selective channel activity (*20*, *21*). Interactions of the protonated (cationic) side chain of His37 with the indole ring of Trp41 on an adjacent helix are believed to play a critical role in the channel gating (*15*, *22–25*). Very recently, atomic-resolution structures including side chain orientations have been solved for M2-TMP and its analogs by NMR spectroscopy in micellar solution (*26*) and by X-ray diffraction in a co-crystal with detergent (*27*). These structural data broadly support the models for the A/M2 proton channel proposed so far, though some differences are apparent between the NMR and X-ray structures.

Influenza B virus also possesses a channel-forming protein (called BM2) activated at acidic pH and required for the virus replication (*28–33*). The BM2 protein is composed of 109 amino acid residues and its single hydrophobic segment (residues 7−25) is considered to be buried in the membrane (*30*). Comparison of the amino acid sequence between A/M2 and BM2 reveals a common motif of HxxxW in the transmembrane domain (Fig. 1) (*31*). Since His37 and Trp41 in the HxxxW motif of A/M2 are essential for the proton channel activity as noted above, the corresponding His−Trp pair (His19 and

*Present address: Division of Pharmacy, Medical and Dental Hospital, Niigata University, 1-754 Asahimachi-dori, Niigata 951-8520, Japan.
†To whom correspondence should be addressed. Tel: +81-22-795-6855, Fax: +81-22-795-6855,
E-mail: takeuchi@mail.tains.tohoku.ac.jp

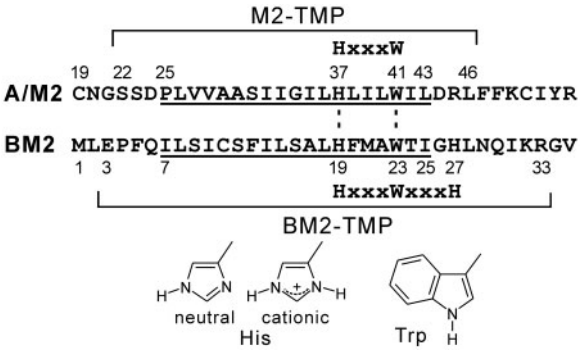

Fig. 1. **Comparison of the amino acid sequences between the A/M2 and BM2 proteins in the N-terminal region including the putative transmembrane hydrophobic segment (underlined).** The sequence data were taken form the UniProtKB/Swiss-Prot database. M2-TMP and BM2-TMP are model peptides representing the putative transmembrane domain. The HxxxW motif is common to A/M2 and BM2, while the WxxxH sequence is unique to BM2. The structures of the His imidazole ring in the neutral and cationic (protonated) states and of the Trp indole ring are also depicted.

Trp23) in BM2 is also expected to play an important role in the proton channel. Actually, the mutation of His19 to Cys abolishes the channel activity and the Trp23→Cys mutation reduces the proton selectivity (*31*). Recent biochemical studies have strongly suggested that the BM2 channel is also tetrameric (*34*), and several residues including His19 and Trp23 are located in or near the channel lumen (*35*). Despite the similarity between A/M2 and BM2, the BM2 channel differs from the A/M2 channel in some electrophysiological properties (*31*). Furthermore, the BM2 channel is not inhibited by the antiviral drug amantadine, unlike the A/M2 channel (*31*). The differences in properties between A/M2 and BM2 are not unreasonable because the amino acid sequence shows little homology except the HxxxW motif (Fig. 1). In contrast to the A/M2 proton channel, information on the structure and mechanism of the BM2 proton channel is very limited at present.

In this study, we have examined the activity and structure of a 31-mer peptide (BM2-TMP) incorporated into lipid liposomes. BM2-TMP includes the putative transmembrane domain of BM2 (Fig. 1) and may be used to study the mechanism of the BM2 channel without interference from the non-transmembrane regions. Special focus has been placed on His19 and Trp23 in the HxxxW motif and additionally on His27, which is unique to BM2 and has a possibility of WxxxH-type interaction with Trp23 (*36*). Assays using a pH-sensitive fluorophore entrapped in peptide-incorporated liposomes have shown that BM2-TMP forms a transmembrane proton channel, which is activated at acidic pH with a midpoint of transition at pH 6.4 ± 0.1. The channel activity is almost abolished by the His19→Ala (H19A) mutation, while it is reduced partially by the His27→Ala (H27A) mutation. The Trp23→Phe (W23F) substitution loses the proton selectivity of the channel. Circular dichroism (CD), fluorescence and Raman spectra of wild-type and mutated BM2-TMP have revealed structural changes of the channel at pH ~6.5 and ~7.6, which are linked with the protonation and concomitant cation−π interaction with Trp23 of the His19 and His27 imidazole rings, respectively. Taken together, it is suggested that His19 triggers the channel opening and His27 enhances the channel activity, both through cation−π interactions with Trp23.

EXPERIMENTAL PROCEDURES

Materials—BM2-TMP (Glu^3-Pro-Phe-Gln-Ile-Leu-Ser-Ile-Cys-Ser-Phe-Ile-Leu-Ser-Ala-Leu-His^{19}-Phe-Met-Ala-Trp^{23}-Thr-Ile-Gly-His^{27}-Leu-Asn-Gln-Ile-Lys-Arg^{33}) and its mutants (H19A, W23F and H27A) were custom-synthesized by Sigma Genosys. The peptides were purified by HPLC on a reversed-phase column (Nacalai Tesque, 5C18-AR-300) with a 50−90% linear gradient of acetonitrile in 0.1% (v/v) trifluoroacetic acid, followed by conversion to the hydrochloride salt in 100 mM hydrochloric acid. The purified peptides were identified by high-resolution mass spectrometry and stored in a freezer as lyophilized powder. The concentrations of BM2-TMP and its H19A and H27A mutants were determined from the UV absorption intensity of Trp at 280 nm ($\varepsilon_{280} = 5{,}500\ M^{-1}cm^{-1}$) (*37*). For the W23F mutant, the concentration was determined by using the relative intensity of an N-deuterated histidine Raman band at 1408 cm^{-1} against a water (D_2O) Raman band at 1204 cm^{-1} in acidic D_2O solution (*38*). 1-Palmitoyl-2-oleoyl-*sn*-glycero-3-phosphoethanolamine (POPE) and 1-palmitoyl-2-oleoyl-*sn*-glycero-3-[phospho-L-serine] (POPS, sodium salt) were purchased from Avanti Polar Lipids and used as received. Dithiothreitol (DTT), valinomycin, pyranine and *p*-xylene-bis-pyridinium bromide (DPX) were purchased from Sigma-Aldrich and used without further purification.

Calibration of the Fluorescent pH Indicator Pyranine—Pyranine is a water-soluble, membrane-impermeable compound and can be used as a probe for monitoring the pH in the internal compartment of liposomes (*39*, *40*). The 510-nm fluorescence intensity of pyranine excited at 460 nm (I_{460ex}) strongly depends on pH, whereas that excited at 415.5 nm ($I_{415.5ex}$) is independent of pH. Thus, the pH around the pyranine molecule can be determined from the intensity ratio $I_{460ex}/I_{415.5ex}$. A calibration curve between the pH and $I_{460ex}/I_{415.5ex}$ was obtained by recording the fluorescence excitation spectra of pyranine in a pH range of 3.96−9.84. The pyranine solution (10 nM) was kept at 5°C and supplemented with K_2HPO_4 (12 mM), K_2SO_4 (50 mM) and POPE/POPS liposomes (20 μM in total lipid) to make the solution conditions close to those of the channel activity assay where the pyranine fluorescence was actually utilized. The solution pH was adjusted by the addition of concentrated H_2SO_4 or KOH. The obtained calibration curve is shown in Supplementary Material (Fig. S1).

Preparation of Peptide-incorporated Liposomes—Prior to incorporation of the peptide into lipid membranes, the peptide was incubated in H_2O/2,2,2-trifluoroethanol (1:1, v/v) at 60°C for 40 min with a 40-fold excess of DTT, and then the solvent was removed by evaporation (*41*). This treatment was made to disrupt possible intermolecular disulphide linkages at Cys11 formed

by autoxidation. All the sample manipulations after the DTT reduction were performed under an atmosphere of high-purity argon. The reduced peptide was co-dissolved with 20–320 equivalents (in total lipid) of POPE/POPS (1:1) in chloroform/methanol (1:1, v/v). For the samples of channel activity assays, the K^+-ionophore valinomycin (0.2 mol% of the total lipid) was added to the solution. The peptide–lipid mixture solution was spread as a thin layer onto the wall of a round-bottom flask by drying under vacuum. Excess drying time (>24 h) was taken to ensure complete removal of the solvent. The dried lipid film was hydrated under vortexing with (i) 50 mM aqueous K_2SO_4 supplemented with 2 mM pyranine for examining the channel activity, (ii) deionized water for CD and fluorescence spectral measurements or (iii) 1.25 mM aqueous KNO_3 (an internal intensity standard) for Raman spectral measurements. The lipid suspension containing multilamellar liposomes was sonicated using an ultrasonic generator with a tip probe (Nihonseiki, US-50) until the solution appeared to be optically transparent. Titanium particles from the tip probe and a trace of large multilamellar liposomes were removed by centrifugation (1,000*g*, 20 min). The hydration and sonication were performed at 35°C, about 15°C above the gel-to-liquid-crystalline phase transition temperature (~20°C) of the POPE/POPS lipid bilayer (*42*). When pyranine was added to the hydration solvent, the pyranine molecules untrapped in the liposomes were removed by gel-filtration on a desalting column (Amersharm Bioscience, PD-10).

Assay of Proton Channel Activity—The proton channel activity was assayed by monitoring the change of pH inside the peptide-incorporated liposome upon drop of the pH outside the liposome. The drop of the external pH was made by a rapid injection of a 250 μl liposome suspension loaded in a syringe into a 2,250 μl acidic external medium in a screw-capped quartz cell equipped with a magnetic stirrer. The liposome suspension (containing 0.625 μM peptide, 200 μM lipid, 50 mM K_2SO_4, 0.4 μM valinomycin and pyranine) was prepared as described above and its pH was adjusted to be 5.5–8.5 by adding aliquots of H_2SO_4 or KOH. The pH equilibration in the liposome suspension was accelerated by incubation at room temperature with an aid of valinomycin that allows K^+ counterflow through lipid membranes against the proton flow through channels (*43*, *44*). The external medium was 50 mM aqueous K_2SO_4 supplemented with DPX (1 mg/ml), a quencher of pyranine fluorescence, to suppress the fluorescence emission from any pyranine molecules outside the liposomes. The pH of the external medium was adjusted to be ~4.5 by the addition of aliquots of concentrated H_2SO_4 (10–30 μM excess in proton concentration compared to the liposome suspension). The quartz cell used as a reaction vessel was thermostated at 5°C and the liposome suspension was also cooled at 5°C prior to the injection. The low temperature condition was employed to minimize the proton permeation through lipid membranes that might interfere the proton flow through the channel (*45*).

The pH in the internal compartment of liposomes (pH_i) was monitored by using the fluorescence from the pyranine molecules trapped within the liposome. Immediately after the injection of the liposome suspension into the external medium, the intensity at 510 nm of the fluorescence excited at 460 nm (I_{460ex}) was recorded for 100 s with an interval of 0.2 s. In the next run, we changed the excitation wavelength to 415.5 nm and the 510-nm fluorescence intensity ($I_{415.5ex}$) was recorded in the same way as I_{460ex} by using another identical sample. A possible small difference in pyranine content between the two samples of paired runs was corrected by comparing the pH-independent $I_{415.5ex}$ values recorded at the end of individual runs. The pH_i at each time point (t) of reaction was determined from the observed $I_{460ex}/I_{415.5ex}$ ratio by using the calibration curve (Fig. S1), and the proton concentration in the internal liposome compartment ($[H^+]_i$) was calculated from the pH_i value. Since the progress curve of $[H^+]_i$ suggested an initial burst of proton influx followed by a slow linear permeation, the $[H^+]_i$ data were fitted to a sum of exponential and linear functions (*46*):

$$[H^+]_i = [H^+]_i^0 + v_s(t-\delta) + (v_i - v_s)(1/k)\{1 - \mathrm{Exp}[-k\,(t-\delta)]\} \quad (1)$$

where $[H^+]_i^0$ is the initial value of $[H^+]_i$, v_i is the initial velocity of the $[H^+]_i$ change, v_s is the velocity of the linear component in the $[H^+]_i$ change, k is the rate constant of the exponential component and δ is a possible time lag. Since the initial rapid increase of $[H^+]_i$ is ascribed to a proton influx through channels, the proton conductance G at the beginning of the reaction may be defined by the initial velocity of proton influx (v_i) divided by the proton concentration difference across the channel:

$$G = v_i/([H^+]_e - [H^+]_i^0) \quad (2)$$

Here, $[H^+]_e$ is the proton concentration in the external medium after injection of the liposome suspension. Since the total volume of the internal liposome compartments was estimated to be much smaller than the volume of the external medium, only a very small fraction of the protons in the external medium were thought to flow into the liposome. Accordingly, we assumed that $[H^+]_e$ remained virtually constant throughout the reaction and calculated the value of $[H^+]_e$ from the pH of the external medium after each run of the assay.

The proton conductance assays were carried out at peptide/lipid ratios of 1/320 and 1/160, which gave substantially identical results. The data to be reported in this article are those obtained at the 1/320 ratio, because the pH change due to proton conductance became slower and more manageable at lower peptide/lipid ratios.

Samples for Spectral Measurements—Since higher peptide/lipid ratios gave better quality spectra, we prepared the samples for CD, fluorescence and Raman spectral measurements at a peptide/lipid ratio of 1/20. (CD and fluorescence spectra recorded at a lower peptide/lipid ratio of 1/80 were not much changed from those at 1/20, though the signal-to-noise ratios were somewhat reduced.) Spectral measurements were carried out in a pH range from alkaline to acidic. To set the pH of the sample to a desired value, an aliquot of the liposome suspension prepared by using deionized water (or supplemented with 1.25 mM KNO_3) as hydration solvent was

mixed with the same volume of K_2HPO_4 (20 mM)/citric acid (10 mM) buffer at pH 4.5–8.0 or of Tris (20 mM)/citric acid (10 mM) buffer at pH 7.5–9.5. The actual pH value of the solution was measured after mixing. The K^+ concentration in the buffer was adjusted to be constant (20 mM) by adding KCl. The final concentration of the peptide in the liposome suspension was 25 μM. For the samples of Raman measurements, the peptide concentration was raised to 100 μM by increasing the initial amount of peptide used for the preparation of liposome and by changing the mixing ratio of liposome suspension and buffer.

Spectral Acquisition—CD spectra of peptide-incorporated liposomes were recorded on a Jasco J-820 spectropolarimeter. The CD spectrum of peptide-free liposome was also recorded separately in the same cell and subtracted from the spectra of peptide-incorporated liposomes. The CD intensity was expressed as molar ellipticity [θ] per amino acid residue. Fluorescence spectra were recorded on a Jasco FR-6500 spectrofluorometer. Background signals due to buffer were subtracted from the spectra of peptide samples. Raman spectra were excited with 229-nm continuous wave radiation from an intra-cavity frequency-doubled Ar^+ laser (Coherent, Innova 300 FReD) and recorded on a UV Raman spectrometer (Jasco, TR-600UV) equipped with a CCD detector (Princeton Instruments, LN/CCD-1152). A spinning cell was used to minimize the sample degradation by laser irradiation, of which the power was kept as low as 0.3 mW at the sample point. Wavenumber calibration was effected by using the Raman spectrum of a cyclohexanone–acetonitrile mixture (1:1, v/v), and peak wavenumbers of sharp Raman bands were reproducible to within $\pm 1\,cm^{-1}$. The cells used for the CD, fluorescence and Raman spectral measurements were sealed with a paraffin film or a silicon rubber plug after filling with the sample under an atmosphere of Ar. All spectral data were acquired at room temperature.

Analysis of pH Dependence—CD, fluorescence and Raman spectra as well as the proton conductance *G* showed pH-dependent changes. To obtain the pH at the midpoint of transition (p*K*), the pH-dependent data were analysed by using a Hill equation (*15*, *47*):

$$Y(\mathrm{pH}) = a/\{1 + 10^{h(\mathrm{pH}-\mathrm{p}K)}\} + b \qquad (3)$$

where *Y*(pH), *a*, *h* and *b* stand for a pH-dependent quantity, its amplitude, a Hill coefficient and a pH-independent constant, respectively. The values of the parameters including p*K* were determined by least-squares fitting to the experimental data. For a biphasic transition, a sum of two Hill equations with different p*K* values was used.

RESULTS

Proton Channel Activity—The proton channel activity of BM2-TMP was assayed by incorporating the peptide into POPE/POPS membranes, which had been shown to be suitable for reconstituting A/M2 proton channels (*13*). The peptide-containing liposome suspension was injected into a more acidic external medium and the change of the pH in the internal liposome compartment (pH_i) was monitored at 5°C by using the pyranine fluorescence. Figure 2 compares the time courses of pH_i change observed for wild-type BM2-TMP and its H19A, H27A and W23F mutants. The data in the absence of peptide are also shown for comparison. In obtaining the assay data in Fig. 2, the pH of the liposome suspension to be injected (the pH of channel preparation) was set to be 6.38 ± 0.02 and that of the external medium was so adjusted that the external pH after the injection of liposomes (pH_e) became 4.80 ± 0.04.

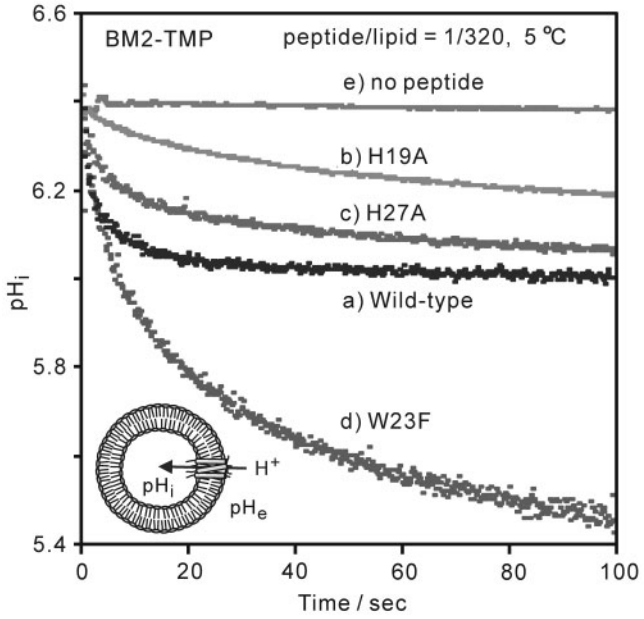

Fig. 2. **Time-dependent change of the pH in the internal liposome compartment (pH_i) observed for (a) wild-type BM2-TMP and its (b) H19A, (c) H27A and (d) W23F mutants incorporated into POPE/POPS liposomes at a peptide/lipid ratio of 1/320.** The data in the absence of peptide (e) are also shown for comparison. The reaction was started by injecting a liposome suspension (250 μl, pH 6.38 ± 0.02) into an external medium (2,250 μl, pH 4.80 ± 0.04 after mixing), and the pH_i value was determined from the fluorescence intensity of pyranine recorded with a time interval of 0.2 s. The liposome suspension contained K_2SO_4 (50 mM), valinomycin (0.2 mol% of the lipid) and pyranine (inside the liposome), whereas the external medium contained K_2SO_4 (50 mM) and DPX (1 mg/ml). The reaction was carried out at 5°C in an air-tight quartz cell filled with Ar gas.

In the absence of BM2-TMP, the pH_i stays constant around its initial value (curve e in Fig. 2), indicating that proton permeation through liposomal membranes is negligible under the present assay conditions. This is probably because the assay temperature (5°C) is much lower than the gel-to-liquid-crystalline phase transition temperature (~20°C) of the POPE/POPS membrane (*42*), and the proton permeation is inhibited by the tightly packed hydrocarbon chains of the lipid in the gel phase membrane (*45*).

In the presence of wild-type BM2-TMP, the pH_i exhibits a rapid exponential decay for about 20 s, followed by a very slow linear decrease continuing for a long time (curve a). The initial rapid decrease of pH_i evidences that BM2-TMP forms a proton channel in the liposomal membrane. The approximate bottoming of pH_i

around 6.0 (1.2 pH unit above pH_e) at about 20 s may be ascribed to a buildup of transmembrane electrical potential opposing further proton influx into the liposomal compartment. On the other hand, the slow decrease of pH_i observed at later stages is likely to reflect a gradual dissipation of the transmembrane electrical potential, probably due to a counterflow of K^+ from the liposome interior to the external medium. A possible K^+ carrier is valinomycin added in the preparation of liposome. Although valinomycin, a large dodecadepsipeptide, is unable to diffuse in the highly ordered lipid membrane in the gel phase (*48*, *49*), it may be able to diffuse, though slowly, in locally disordered regions of the membrane around the incorporated peptide molecules. Another possibility of the K^+ counterflow is a weak activity of BM2-TMP as a K^+ channel. Although the K^+ conductance is very low (10^{-6}–10^{-7} of the proton conductance) for the A/M2 channel (*44*, *50*), it might be higher for the BM2-TMP channel. No matter what is the origin of the slow linear decrease of pH_i at later stages, the initial rapid change of pH_i may serve as a measure of the proton channel activity.

The proton channel activity of BM2-TMP largely diminishes upon mutation of His19 to Ala (curve b in Fig. 2). The decrease of pH_i is very slow for the H19A mutant compared to the wild-type, indicating that the H19A mutant does not form an effective proton channel. This observation is consistent with the previous finding that the mutation of His19 to Cys in the full-length BM2 protein abolishes the proton channel activity (*31*, *35*). His19 is a residue composing the HxxxW motif in the transmembrane domain (Fig. 1) and it may play an important role in the channel activity. On the other hand, the H27A mutant exhibits an initial pH_i decay ascribable to channel formation (curve c), though its velocity is significantly lowered compared to that of the wild-type peptide. His27 may not be essential for the proton channel activity.

In sharp contrast to the His mutants, the mutation of Trp23 to Phe amplifies the pH_i change to a large extent, in particular at later stages of the reaction (curve d in Fig. 2). The pH_i continues to decrease toward the pH_e value (~4.8) and no buildup of transmembrane electrical potential is seen. This observation suggests that the W23F mutant forms a channel, which allows both the influx of proton into the liposome and the efflux of ions such as K^+ out of the liposome, without forming imbalance of electrical potential between the inside and outside of the liposomal membrane. Analogous loss of proton selectivity has been observed for the Trp23→Cys mutant of BM2 by electrophysiology (*31*). Trp23 may be essential for forming a stable proton-selective channel.

pH Dependence of Proton Conductance—To quantitatively compare the proton channel activities of wild-type and mutated BM2-TMP at varied pH values, we defined the proton conductance G by Equation 2. To obtain the G value, we need to plot the proton concentration inside the liposome ($[H^+]_i$) as a function of time. The inset of Fig. 3 shows the change of $[H^+]_i$ (left scale) calculated from the observed pH_i values (right scale) of wild-type BM2-TMP shown in Fig. 2. The biphasic change of $[H^+]_i$ was fitted to Equation 1 to obtain the initial velocity v_i,

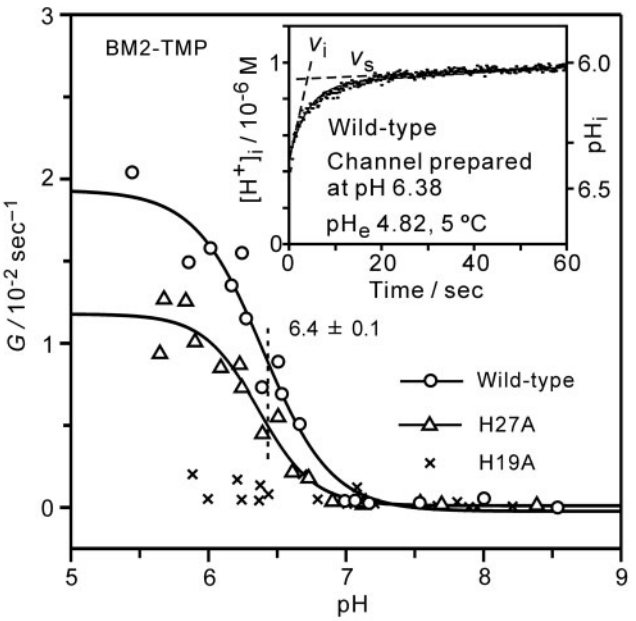

Fig. 3. **Plots of the proton conductance G as a function of the pH of channel preparation (the pH of liposome suspension before injection into an external medium) for transmembrane channels formed by wild-type BM2-TMP and its H19A and H27A mutants (peptide/lipid ratio, 1/320).** The dashed vertical line indicates the midpoint of transition. The uncertainty given is twice the standard error. In the inset, the proton concentration in the liposomal compartment ($[H^+]_i$) is plotted as a function of time for a typical run of the assay using wild-type BM2-TMP. A POPE/POPS liposome suspension (250 μl) containing BM2-TMP (0.625 μM) was injected into an external medium (2,250 μl), and $[H^+]_i$ was calculated from the pH_i value determined from the pyranine fluorescence. The liposome suspension contained K_2SO_4 (50 mM), valinomycin (0.2 mol% of the lipid) and pyranine (inside the liposome), whereas the external medium contained K_2SO_4 (50 mM) and DPX (1 mg/ml). The pH of channel preparation for the data in the inset was 6.38 and the external pH (pH_e) was 4.82. The reaction was performed at 5°C under an atmosphere of Ar. The solid curve in the inset shows a fit of the $[H^+]_i$ data to Equation 1 and a broken line indicates v_i, from which the proton conductance G was calculated using Equation 2.

and the conductance G was calculated from the v_i value by using Equation 2. Measurements of G values were performed for wild-type and mutated BM2-TMP with varying the pH of liposome suspension before injection (the pH of channel preparation) in a 5.5–8.5 range and keeping the pH_e at 4.75 ± 0.20. The obtained G values are plotted against the pH of channel preparation in the main part of Fig. 3.

For wild-type BM2-TMP, the channel is activated at acidic pH with a midpoint of transition at pH 6.4 ± 0.1, and no significant conductance is observed at alkaline pH above 7.5 as shown in Fig. 3. (The data in the inset of Fig. 3 corresponds to the data point at pH 6.38 in the main part of Fig 3.) The G value depends on the pH of channel preparation but not on pH_e (kept constant) nor pH_i (approaching pH_e with the progress of reaction). This is probably because the channel state, open or closed, is determined by the pH of the liposome suspension before injection into the external medium, at least at the

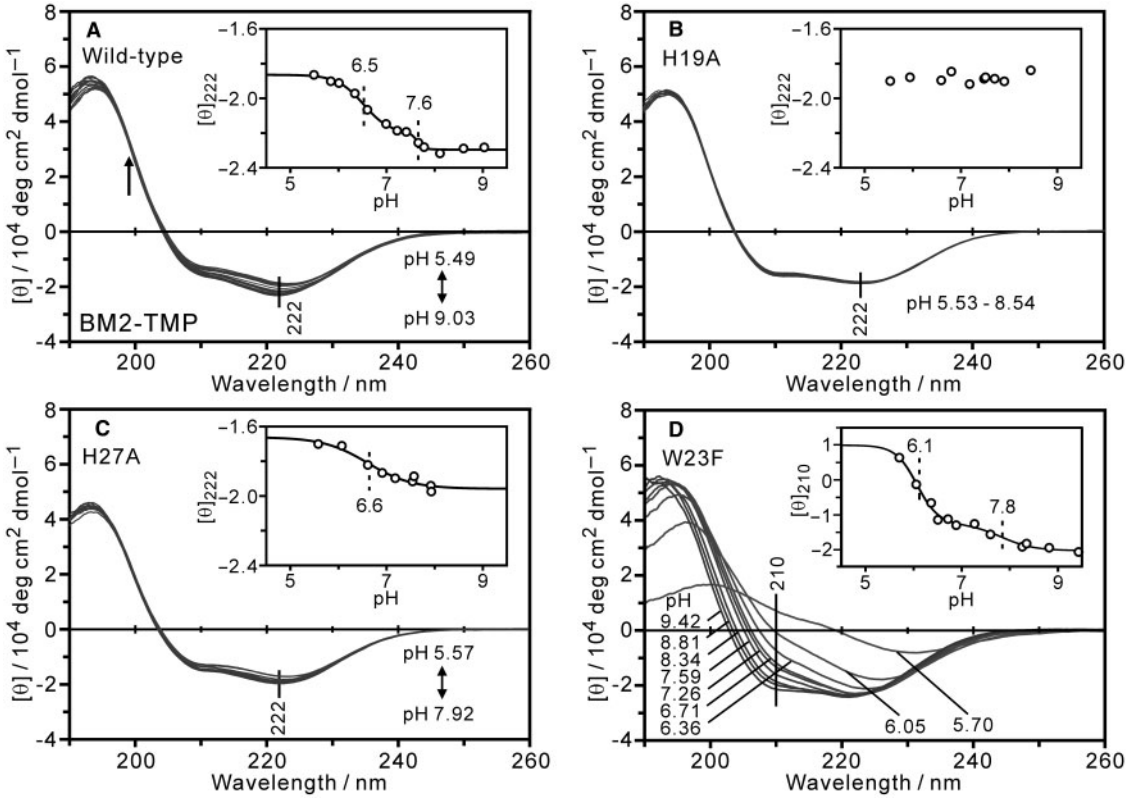

Fig. 4. **CD spectra of (A) wild-type BM2-TMP and its (B) H19A, (C) H27A and (D) W23F mutants incorporated into POPE/POPS liposomes (peptide/lipid molar ratio, 1/20).** The pH of the sample was varied from alkaline to acidic as indicated and the spectra were recorded at room temperature. An upward arrow at 199 nm in (A) indicates the position of an isodichroic point. In the inset of each panel, the molar ellipticity at 222 or 210 nm ($[\theta]_{222}$ or $[\theta]_{210}$) is plotted against pH. The dashed vertical line indicates the midpoint of transition.

beginning of the reaction. If the channel state is immediately affected by the environmental pH (pH_e and pH_i) during the reaction, significant proton conductance would be observed even for the channels prepared at alkaline pH, because injection of the liposome into the external medium causes exposure to acidic pH_e that activates the channel. Actually, however, the channel conductance determined from the initial velocity v_i is negligibly small for the channels prepared at alkaline pH (see Fig. 3). A recent X-ray diffraction study has proposed a significant difference in helix arrangement between the open and closed states of the A/M2 channel (*27*). The open–closed transition of the BM2 channel may also require a rearrangement of the transmembrane helices, which involves the surrounding lipid molecules. The tightly packed POPE/POPS membrane in the gel phase at 5°C may contribute to delaying the structural transition of the BM2-TMP channel between the open and closed states. Actually, at temperatures higher than the lipid phase transition temperature, the proton influx is accelerated, in particular at later stages of the reaction, as shown in Supplementary Material (Fig. S2).

In contrast to wild-type BM2-TMP, the H19A mutant shows no significant conductance throughout the pH range examined (Fig. 3), again indicating an essential role of His19 in the proton conductance by BM2-TMP. Upon mutation of His27 to Ala, the maximum conductance of wild-type BM2-TMP observed at acidic pH is reduced to about 60%, whereas the pH of the transition midpoint is not affected by the mutation (Fig. 3). His27 may not be involved in the channel opening mechanism, but the residue is likely to contribute to elevation of the channel activity.

pH Dependence of CD Spectra—To examine the structure of the BM2-TMP channel, we have recorded CD spectra of BM2-TMP and its mutants incorporated into POPE/POPS liposomes. Figure 4A shows the CD spectra of wild-type BM2-TMP at pH 5.49–9.03. In all the spectra, a double-minimum is observed at 210/222 nm, indicating that the peptide takes a predominantly α-helical structure in the pH range examined (*51*). Close examination of the spectra reveals a small pH dependence: the higher the pH, the stronger the signal at 222 nm. Since the isodichroic point at 199 nm (indicated with an arrow in the figure) is significantly above the zero-intensity horizontal axis, the CD spectral change is ascribed to a change in spectral shape but not to a simple change in overall intensity. The inset of Fig. 4A shows the plot of the molar ellipticity at 222 nm ($[\theta]_{222}$) as a function of pH. A weak transition and a more distinct transition are observed at pH 7.6 and 6.5, respectively. These small changes of the CD spectra may be due to changes in structure associated with the protonation of His19 and/or His27 because the other residues of BM2-TMP are unlikely to have a pK_a around 7.6 or 6.5. As expected, mutation of the His residues significantly

affects the pH-dependence of the CD spectrum. Both transitions at pH 7.6 and 6.5 disappear in the H19A mutant (Fig. 4B), while only one transition is seen at pH 6.6 in the H27A mutant (Fig. 4C). Thus, the transition at pH 7.6 observed for the wild-type may be related to the protonation of His27, and the transition at pH 6.5 is mainly associated with the protonation of His19. The absence of pH-dependent CD change in the H19A mutant (Fig. 4B) implies that the His19→Ala mutation introduces rigidity into the channel structure.

The CD intensity at 222 nm is usually regarded as a measure of α-helical content (*51*). In some proteins, however, interactions of Trp with the surroundings also give CD signals around this wavelength (*52*). Furthermore, the negative CD band at 223 nm of M2-TMP of influenza A virus has been reported to increase in magnitude upon formation of a tetramer or binding of amantadine, and to decrease with decrease of pH as observed here for BM2-TMP (*53*). Therefore, it is difficult to precisely define the origin of the CD intensity change around 222 nm. Nevertheless, the CD spectral changes observed here for BM2-TMP may be ascribed to some structural changes associated with the protonation of the His residues.

The CD spectra of the W23F mutant are largely different from those of the wild-type and the H19A and H27A mutants (Fig. 4D). Although the presence of a double-minimum at pH > 8 indicates dominance of an α-helical structure (*51*), the CD spectrum significantly deviates from that of a typical α-helical structure in going to pH 6, and finally the peptide takes an unknown structure below pH 6. In the inset of Fig. 4D, the molar ellipticity at 210 nm ($[\theta]_{210}$), where the largest intensity change was observed, is plotted against pH. The plot clearly shows that the decay of the α-helical structure begins around pH 7.8 and completes below pH 6. The beginning of the helix unfolding may be associated with the protonation of His27 and its acceleration may be related to the additional protonation of His19. It is likely that Trp23 plays a role in maintaining the channel structure by reducing the electrostatic repulsion between the protonated His residues. The instability of the α-helix in the W23F mutant implies a loosened channel structure for this mutant, being consistent with the loss of proton selectivity (Fig. 2).

Trp Fluorescence and His Protonation—Trp emits fluorescence when excited with UV light. Figure 5A shows the emission spectra of BM2-TMP incorporated into POPE/POPS liposomes and excited at 280 nm. The pH of the sample was varied between 4.98 and 8.91. Each spectrum is dominated by a strong emission band at 338 nm assignable to the fluorescence of Trp23 (*54*). Additional weak peaks above 400 nm (414 and 437 nm) are ascribed to phosphorescence (*55*), which was not quenched by atmospheric oxygen because the liposome sample was kept under an Ar atmosphere. The Trp fluorescence at 338 nm decreases in intensity with decrease of pH without any change in peak position. The invariable peak position suggests that the intensity decrease is due to a simple quenching mechanism that does not involve significant changes in environmental polarity and/or mobility (*54*). The plot of intensity at

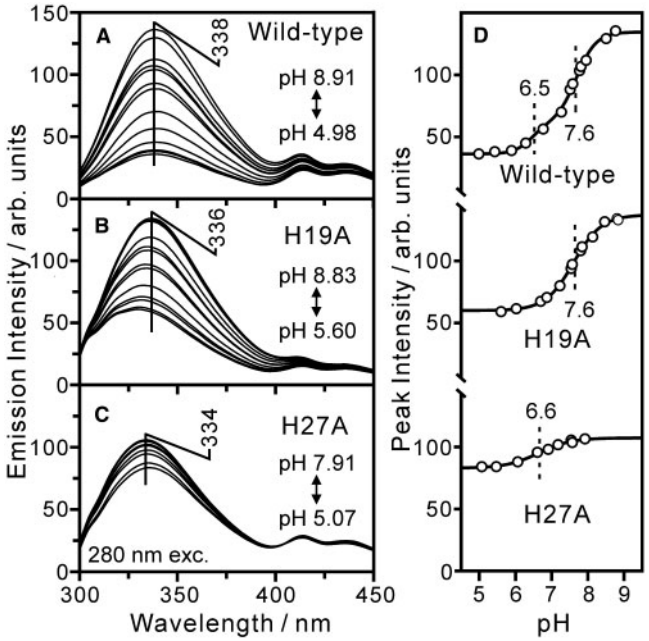

Fig. 5. **Emission spectra of (A) wild-type BM2-TMP and its (B) H19A and (C) H27A mutants incorporated into POPE/POPS liposomes (peptide/lipid molar ratio, 1/20) and excited at 280 nm.** The pH of the sample was varied from alkaline to acidic as indicated. The strong band peaking at 334–338 nm is due to fluorescence from Trp23 and the weak bands between 400 and 450 nm are ascribed to phosphorescence. In the right panel (D), the peak intensity of the fluorescence band is plotted against pH. The dashed vertical line indicates the midpoint of transition.

338 nm against pH shows two steps of quenching at pH 7.6 (strong) and 6.5 (weak) (Fig. 5D), of which the former disappears in the H27A mutant (Fig. 5C and D) and the latter disappears in the H19A mutant (Fig. 5B and D). Accordingly, the strong quenching at pH 7.6 is related to the protonation of His27 and the weak quenching at pH 6.5 to the protonation of His19. The pK_a values of His19 and His27 obtained from the Trp23 fluorescence quenching is identical to those obtained from the pH-dependent CD spectral changes in Fig. 4.

Analogous quenching of Trp fluorescence by a protonated His residue has been reported for the Trp41–His37 pair of A/M2 (*24*), the Trp94–His18 pair of the microbial ribonuclease barnase (*56*), and the W–H pair in a model peptide for the WxxxH motif (*36*). The fluorescence quenching may be ascribed to direct interactions of the protonated (cationic) imidazole ring of His with the indole ring of Trp in the excited electronic state (*54*). To interact in the excited state, the His imidazole ring is required to be located near the indole ring of Trp as found for barnase by X-ray diffraction (*57*). Thus, the pH-dependent quenching of Trp23 fluorescence strongly suggests that the protonated imidazole rings of His19 and His27 are in close proximity with the Trp23 indole ring. Generally, short-distance electrostatic interactions between a cation and a π-electron system is categorized as a cation–π interaction, which is recognized as an important non-covalent force that influences the

structures and functions of a variety of molecules including proteins (*58*, *59*). It is highly probable that the cation−π interaction takes place between His27 and Trp23 below pH 7.6 and between His19 and Trp23 below pH 6.5.

Trp Raman Spectra—UV resonance Raman spectroscopy is a useful tool for obtaining information on the structure and interaction of Trp as demonstrated in a previous study on the M2-TMP proton channel (*15*). To obtain structural information on Trp23, we have recorded Raman spectra of the BM2-TMP channel reconstituted into POPE/POPS liposomes. The excitation wavelength employed (229 nm) is close to the λ_{max} (220 nm) of the Trp B_b absorption band, and vibrational Raman bands of Trp, in particular those resonant with the B_b transition (*60*), are expected to be selectively enhanced.

Figure 6A shows the Raman spectra of wild-type and mutated BM2-TMP under acidic and alkaline conditions.

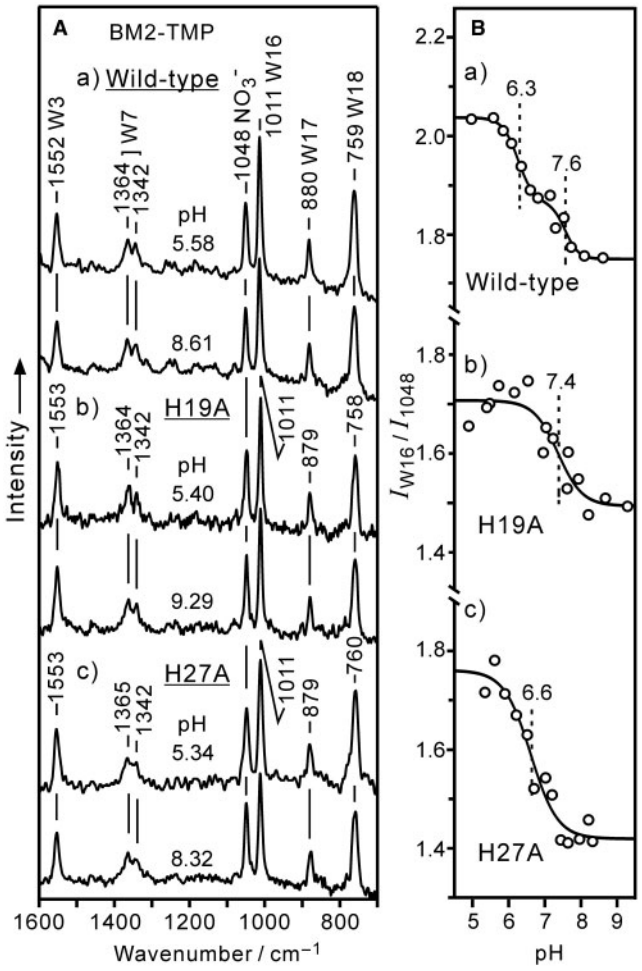

Fig. 6. **(A) Raman spectra of (a) wild-type BM2-TMP and its (b) H19A and (c) H27A mutants incorporated into POPE/POPS liposomes (peptide/lipid molar ratio, 1/20) at acidic and alkaline pH as indicated.** The Raman scattering was excited at 229 nm. The 1048 cm^{-1} band is due to NO_3^- added as an internal intensity standard. All the other bands are assigned to Trp23. (B) The peak intensity ratio of the W16 and 1048 cm^{-1} bands (I_{W16}/I_{1048}) plotted against pH. The dashed vertical line indicates the midpoint of transition.

Except the 1048 cm^{-1} band of NO_3^- added as an internal intensity standard, all the Raman bands in the spectra are assigned to Trp indole ring vibrations as indicated with a label W followed by its mode number (*61*). Comparison of the spectra under acidic and alkaline conditions reveals intensity increases of the B_b-resonant W3, W16, W17 and W18 bands upon acidification. To further examine the pH dependence of the Raman scattering intensity, we have plotted the peak intensity ratio of the W16 band (I_{W16}) against the 1048 cm^{-1} band of NO_3^- (I_{1048}) as a function of pH in Fig. 6B. Wild-type BM2-TMP shows two transitions at pH 7.6 and 6.3 in the I_{W16}/I_{1048} plot, whereas the H19A and H27A mutants exhibit only one transition at pH 7.4 and 6.6, respectively (Fig. 6B). Accordingly, the increase of Trp Raman intensity at pH 7.6, which disappears in the H27A mutant, is ascribed to the protonation of His27, and the other intensity increase at pH 6.3 is attributed to the protonation of His19. The pK_a value of His19 inferred from the Raman spectra (6.3) are slightly lower than those obtained from the CD and fluorescence spectra (6.5), though the difference is within the experimental error (±0.2).

Since UV resonance Raman intensity of Trp is sensitive to its hydrophobic and hydrogen bonding interactions with the environment (*62*, *63*), the increase of the Trp23 Raman intensity upon protonation of His19 and His27 might be ascribed to a change in environment of Trp23. However, such possibility is ruled out because no significant pH dependence is observed in the W7 doublet intensity ratio (a marker of hydrophobic interaction) (*63*, *64*) and in the W17 wavenumber (a hydrogen bonding marker) (*63*, *65*). Alternatively, the intensity change of W16 is consistently explained by assuming cation−π interactions between the His residues and Trp23. It is known that the B_b absorption band of the Trp indole ring undergoes a small red-shift accompanied by a weakening upon cation−π interaction (*15*). As a result of this absorption change, B_b-resonant Raman bands of Trp gain intensity when excited at a slightly longer wavelength (such as 229 nm) than the λ_{max} (220 nm) of the B_b transition (*15*, *66*). The increase of Trp23 Raman intensity observed at pH 7.6 is ascribed to an intensity gain arising from the cation−π interaction between His27 and Trp23, while the intensity increase at pH 6.3 is attributed to the His19−Trp23 cation−π interaction. The Raman spectra in Fig. 6 are consistent with the cation−π interactions between the His and Trp residues suggested by the fluorescence quenching data.

DISCUSSION

We have investigated the activity and structure of the BM2 proton channel by using a model peptide (BM2-TMP) representing the transmembrane domain of the BM2 protein. The results clearly show that BM2-TMP forms a proton channel in POPE/POPS membranes, and the channel is activated at acidic pH as is reported for the full-length BM2 protein (*31*). This finding confirms that the core of the BM2 proton channel is composed of the putative transmembrane region. The channel activity is almost abolished by the His19→Ala mutation, and the

proton selectivity is largely reduced by the Trp23→Phe mutation. On the other hand, the channel activity is decreased but not completely suppressed by the substitution of Ala for His27. The pK_a of the imidazole ring is ~6.5 for His19 and ~7.6 for His27. Upon protonation of His19 and His27, the channel structure slightly changes, and the cation−π interaction takes place between the protonated His imidazole ring and the indole ring of Trp23. The His19−Trp23 cation−π interaction occurs in conjunction with the channel opening at pH 6.4 ± 0.1, while the His27−Trp23 cation−π interaction enhances the activity of the opened channel. Trp23 plays an important role in forming a stable proton-selective channel.

The present findings summarized above strongly suggest that His19 and Trp23, constituting the HxxxW motif in the transmembrane domain, play a key role in the BM2 proton channel as in the case of the A/M2 channel (*15*, *20*–*25*). That is, the protonation of His19 (His37 in A/M2) triggers the channel opening through cation−π interaction with Trp23 (Trp41), which forms a major part of the gate for regulating the proton translocation through the channel lumen. The fundamental mechanism of the channel gating and proton selectivity based on the HxxxW motif appears to be shared by the A/M2 and BM2 channels.

An important difference between A/M2 and BM2 is the presence of His27 on the C-terminal extension of the BM2 transmembrane hydrophobic segment (Ile7−Ile25, Fig. 1). His27 is separated by three intervening residues from Trp23 (a WxxxH sequence), and the side chains of His27 and Trp23 can interact with each other at a distance of one helix pitch or less (<5.4 Å) if the transmembrane helix extends toward the C-terminal side by two or more residues from the last hydrophobic residue (Ile25, Fig. 1) (*36*). Actually, the His27−Trp23 interaction occurs below pH 7.6 as evidenced by the fluorescence and Raman intensity changes of Trp23 (Figs. 5 and 6). This observation raises the possibility that the transmembrane helix is extended to His27 or more. In the atomic-resolution structures solved by NMR spectroscopy and X-ray diffraction (Protein Data Bank accession code, 2RLF and 3BKD) (*26*, *27*), the transmembrane helix of the A/M2 channel is extended toward the C-terminal side, at least by three residues from the last hydrophobic residue (Leu43). Accordingly, it may be reasonable to assume that the transmembrane helix of BM2 is also extended at least to His27. Actually, chemical modification has suggested that His27 is located at the boundary of the transmembrane region (*35*). Figure 7 shows a model for the BM2 channel in the channel open state. In the model, His27 interacts with Trp23 on the same helix through cation−π interaction, whereas Trp23 interacts with His19 on an adjacent helix as in the case of the A/M2 channel (*26*, *27*). The proton is normally conducted from the N-terminal to the C-terminal side (*30*, *31*).

The mutation of His27 to Ala decreased the proton conductance to about 60% of that of the wild-type (Fig. 3), indicating a significant contribution of His27 to the channel activity. This observation is consistent with an electrophysiological report that the His27→Cys mutation of BM2 reduced the channel activity to about 70%

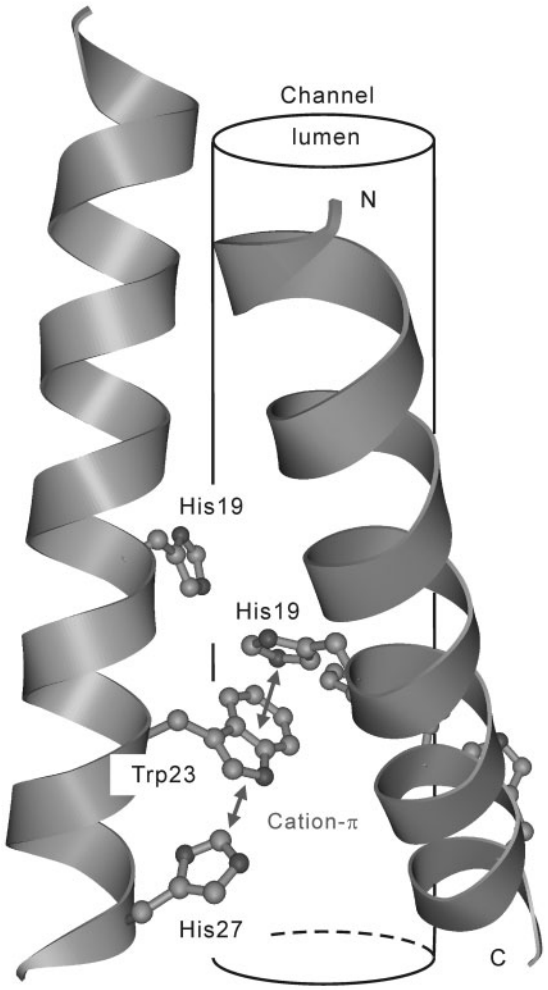

Fig. 7. **Model for the BM2 proton channel in the transmembrane region viewed from a position perpendicular to the channel lumen.** Only two of the four helices surrounding the channel lumen are shown for clarity. The double arrows indicate the His19-Trp23 and His27-Trp23 cation−π interactions. The former interaction triggers the opening of the gate and the latter enhances the channel activity.

(*35*). Since His27 of BM2 corresponds to Arg45 in A/M2 (Fig. 1), it might be thought that the role of His27 can be inferred from the role of Arg45 in the A/M2 channel because the protonated imidazole ring of His27 is analogous to the positively charged guanidinium group (pK_a ~12.5) of Arg45. In the crystalline and solution structures of M2-TMP (or its analogs), Arg45 forms a salt bridge with Asp44 on an adjacent helix and the interhelical interaction is thought to contribute to the stabilization of the four-helix-bundle structure of A/M2 (*26*, *27*). In BM2, however, Gly26 substitutes for Asp44 of A/M2 and no acidic residues that can form a salt bridge with His27 are found in the neighborhood of His27 (Fig. 1). Rather, the fluorescence and Raman spectra indicate an interaction between His27 and Trp23, highly probably on the same helix. Accordingly, it is unlikely that His27 takes part in an interhelical interaction as Arg45 of A/M2 does.

A possible role of His27 in the BM2 channel may be a modification of the position and/or orientation of the indole ring of Trp23 by using the cation−π interaction between the protonated imidazole ring and the indole π-electron system. As the present and previous mutation studies have shown (*31*), Trp23 is a key residue that determines the proton conductivity and selectivity, and even a small change in position and/or orientation of the indole ring would be effective in improving the proton conductance. His27 may be a modifier of the channel activity located near the C-terminal end of the channel lumen. The residue might also be involved in the electrophysiological properties that the BM2 channel is less resistant to the reverse proton flow from the C-terminal to the N-terminal side than the A/M2 channel (*31*). Although the detailed mechanism of the BM2 proton channel remains unclear, the interplay of His19, Trp23 and His27 appears to constitute a major part of the channel machinery.

SUPPLEMENTARY DATA

Supplementary data are available at *JB* online.

ACKNOWLEDGEMENTS

We thank Prof. Lawrence H. Pinto of Northwestern University for suggestion of the amino acid sequence representing the BM2 transmembrane domain.

FUNDING

Japan Society for the Promotion of Science [Scientific Research (B) 16350003] in part.

CONFLICT OF INTEREST

None declared.

REFERENCES

1. Pinto, L.H. and Lamb, R.A. (2007) Controlling influenza virus replication by inhibiting its proton channel. *Mol. BioSyst.* **3**, 18–23
2. Fischer, W.B. and Sansom, M.S.P. (2002) Viral ion channels: structure and function. *Biochim. Biophys. Acta* **1561**, 27–45
3. Pinto, L.H., Holsinger, L.A., and Lamb, R.A. (1992) Influenza virus M_2 protein has ion channel activity. *Cell* **69**, 517–528
4. Takeda, M., Pekosz, A., Shuck, K., Pinto, L.H., and Lamb, R.A. (2002) Influenza A virus M_2 ion channel activity is essential for efficient replication in tissue culture. *J. Virol.* **76**, 1391–1399
5. Chizhmakov, I.V., Geraghty, F.M., Ogden, D.C., Hayhurst, A., Antoniou, M., and Hay, A.J. (1996) Selective proton permeability and pH regulation of the influenza virus M2 channel expressed in mouse erythroleukaemia cells. *J. Physiol.* **494**, 329–336
6. Zhirnov, O.P. (1990) Solubilization of matrix protein M1/M from virions occurs at different pH for orthomyxo- and paramyxoviruses. *Virol.* **176**, 274–279
7. Bui, M., Whittaker, G., and Helenius, A. (1996) Effect of M1 protein and low pH on nuclear transport of influenza virus ribonucleoproteins. *J. Virol.* **70**, 8391–8401
8. Takeuchi, K. and Lamb, R.A. (1994) Influenza virus M_2 protein ion channel activity stabilizes the native form of fowl plague virus hemagglutinin during intracellular transport. *J. Virol.* **68**, 911–919
9. Ohuchi, M., Cramer, A., Vey, M., Ohuchi, R., Garten, W., and Klenk, H.-D. (1994) Rescue of vector-expressed fowl plague virus hemagglutinin in biologically active form by acidotropic agents and coexpressed M_2 protein. *J. Virol.* **68**, 920–926
10. Sugrue, R.J. and Hay, A.J. (1991) Structural characteristics of the M2 protein of influenza A viruses: evidence that it forms a tetrameric channel. *Virol.* **180**, 617–624
11. Sakaguchi, T., Tu, Q., Pinto, L.H., and Lamb, R.A. (1997) The active oligomeric state of the minimalistic influenza virus M_2 ion channel is a tetramer. *Proc. Natl Acad. Sci. USA* **94**, 5000–5005
12. Kochendoerfer, G.G., Salom, D., Lear, J.D., Wilk-Orescan, , R. Kent, S.B.H., and DeGrado, W.F. (1999) Total chemical synthesis of the integral membrane protein influenza A virus M2: role of its C-terminal domain in tetramer assembly. *Biochemistry* **38**, 11905–11913
13. Duff, K.C. and Ashley, R.H. (1992) The transmembrane domain of influenza A M2 protein forms amantadine-sensitive proton channels in planar lipid bilayers. *Virol.* **190**, 485–489
14. Duff, K.C., Kelly, S.M., Price, N.C., and Bradshaw, J.P. (1992) The secondary structure of influenza A M2 transmembrane domain. A circular dichroism study. *FEBS. Lett.* **311**, 256–258
15. Okada, A., Miura, T., and Takeuchi, H. (2001) Protonation of histidine and histidine-tryptophan interaction in the activation of the M2 ion channel from influenza A virus. *Biochemistry* **40**, 6053–6060
16. Pinto, L.H., Dieckmann, G.R., Gandhi, C.S., Papworth, C.G., Braman, J., Shaughnessy, M.A., Lear, J.D., Lamb, R.A., and Degrado, W.F. (1997) A functionally defined model for the M2 proton channel of influenza A virus suggests a mechanism for its ion selectivity. *Proc. Natl Acad. Sci. USA* **94**, 11301–11306
17. Kovacs, F.A., Denny, J.K., Song, Z., Quine, J.R., and Cross, T.A. (2000) Helix tilt of the M2 transmembrane peptide from influenza A virus: An intrinsic property. *J. Mol. Biol.* **295**, 117–125
18. Torres, J. and Arkin, I.T. (2002) C-deuterated alanine: A new label to study membrane protein structure using site-specific infrared dichroism. *Biophys. J.* **82**, 1068–1075
19. Tian, C., Tobler, K., Lamb, R.A., Pinto, L.H., and Cross, T.A. (2002) Expression and initial structural insights from solid-state NMR of the M2 proton channel from influenza A virus. *Biochemistry* **41**, 11294–11300
20. Tang, Y., Zaitseva, F., Lamb, R.A., and Pinto, L.H. (2002) The gate of the influenza virus M2 proton channel is formed by a single tryptophan residue. *J. Biol. Chem.* **277**, 39880–39886
21. Venkataraman, P., Lamb, R.A., and Pinto, L.H. (2005) Chemical rescue of histidine selectivity filter mutants of the M2 ion channel of influenza A virus. *J. Biol. Chem.* **280**, 21463–21472
22. Nishimura, K., Kim, S., Zhang, L., and Cross, T.A. (2002) The closed state of a H^+ channel helical bundle combining precise orientational and distance restraints from solid state NMR. *Biochemistry* **41**, 13170–13177
23. Takeuchi, H., Okada, A., and Miura, T. (2003) Roles of the histidine and tryptophan side chains in the M2 proton channel from influenza A virus. *FEBS Lett.* **552**, 35–38
24. Czabotar, P.E., Martin, S.R., and Hay, A.J. (2004) Studies of structural changes in the M2 proton channel of influenza A virus by tryptophan fluorescence. *Virus Res.* **99**, 57–61
25. Witter, R., Nozirov, F., Sternberg, U., Cross, T.A., Ulrich, A.S., and Fu, R. (2008) Solid-state ^{19}F NMR spectroscopy reveals that Trp41 participates in the gating mechanism of the M2 proton channel of influenza A virus. *J. Am. Chem. Soc.* **130**, 918–924

26. Schnell, J.R. and Chou, J.J. (2008) Structure and mechanism of the M2 proton channel of influenza A virus. *Nature* **451**, 591–595
27. Stouffer, A.L., Acharya, R., Salom, D., Levine, A.S., Di Costanzo, L., Soto, C.S., Tereshko, V., Nanda, V., Stayrook, S., and DeGrado, W.F. (2008) Structural basis for the function and inhibition of an influenza virus proton channel. *Nature* **451**, 596–599
28. Horvath, C.M., Williams, M.A., and Lamb, R.A. (1990) Eukaryotic coupled translation of tandem cistrons: identification of the influenza B virus BM2 polypeptide. *EMBO J.* **9**, 2639–2647
29. Odagiri, T., Hong, J., and Ohara, Y. (1999) The BM2 protein of influenza B virus is synthesized in the late phase of infection and incorporated into virions as a subviral component. *J. Gen. Virol.* **80**, 2573–2581
30. Paterson, R.G., Takeda, M., Ohigashi, Y., Pinto, L.H., and Lamb, R.A. (2003) Influenza B virus BM2 protein is an oligomeric integral membrane protein expressed at the cell surface. *Virol.* **306**, 7–17
31. Mould, J.A., Paterson, R.G., Takeda, M., Ohigashi, Y., Venkataraman, P., Lamb, R.A., and Pinto, L.H. (2003) Influenza B virus BM2 protein has ion channel activity that conducts protons across membranes. *Dev. Cell* **5**, 175–184
32. Hatta, M., Goto, H., and Kawaoka, Y. (2004) Influenza B virus requires BM2 protein for replication. *J. Virol.* **78**, 5576–5583
33. Imai, M., Watanabe, S., Ninomiya, A., Obuchi, M., and Odagiri, T. (2004) Influenza B virus BM2 protein is a crucial component for incorporation of viral ribonucleoprotein complex into virions during virus assembly. *J. Virol.* **78**, 11007–11015
34. Balannik, V., Lamb, R.A., and Pinto, L.H. (2008) The oligomeric state of the active BM2 ion channel protein of influenza B virus. *J. Biol. Chem.* **283**, 4895–4904
35. Ma, C., Soto, C.S., Ohigashi, Y., Taylor, A., Bournas, V., Glawe, B., Udo, M.K., Degrado, W.F., Lamb, R.A., and Pinto, L.H. (2008) Identification of the pore-lining residues of the BM2 ion channel protein of influenza B virus. *J. Biol. Chem.* **283**, 15921–15931
36. Fernández-Recio, J., Vázquez, A., Civera, C., Sevilla, P., and Sancho, J. (1997) The tryptophan/histidine interaction in α-helices. *J. Mol. Biol.* **267**, 184–197
37. Pace, C.N., Vajdos, F., Fee, L., Grimsley, G., and Gray, T. (1995) How to measure and predict the molar absorption coefficient of a protein. *Protein Sci.* **4**, 2411–2423
38. Tasumi, M., Harada, I., Takamatsu, T., and Takahashi, S. (1982) Raman studies of L-histidine and related compounds in aqueous solution. *J. Raman Spectrosc.* **12**, 149–151
39. Kano, K. and Fendler, J.H. (1978) Pyranine as a sensitive pH probe for liposome interiors and surfaces. *Biochim. Biophys. Acta* **509**, 289–299
40. Clement, N.R. and Gould, J.M. (1981) Pyranine (8-hydroxy-1,3,6-pyrenetrisulfonate) as a probe of internal aqueous hydrogen ion concentration in phospholipid vesicles. *Biochemistry* **20**, 1534–1538
41. Okada, A., Miura, T., and Takeuchi, H. (2003) Zinc- and pH-dependent conformational transition in a putative interdomain linker region of the influenza virus matrix protein M1. *Biochemistry* **42**, 1978–1984
42. Epand, R.M. and Lim, W. (1995) Mechanism of liposome destabilization by polycationic amino acids. *Biosci. Rep.* **15**, 151–160
43. Andreoli, T.E., Tieffenberg, M., and Tosteson, D.C. (1967) The effect of valinomycin on the ionic permeability of thin lipid membranes. *J. Gen. Physiol.* **50**, 2527–2545
44. Lin, T. and Schroeder, C. (2001) Definitive assignment of proton selectivity and attoampere unitary current to the M2 ion channel protein of influenza A virus. *J. Virol.* **75**, 3647–3656
45. Bramhall, J. (1987) Conductance routes for protons across membrane barriers. *Biochemistry* **26**, 2848–2855
46. Miura, T., Sasaki, S., Toyama, A., and Takeuchi, H. (2005) Copper reduction by the octapeptide repeat region of prion protein: pH dependence and implications in cellular copper uptake. *Biochemistry* **44**, 8712–8720
47. Markley, J.L. (1973) Nuclear magnetic resonance studies of trypsin inhibitors. Histidines of virgin and modified soybean trypsin inhibitor (Kunitz). *Biochemistry* **12**, 2245–2250
48. Krasne, S., Eisenman, G., and Szabo, G. (1971) Freezing and melting of lipid bilayers and the mode of action of nonactin, valinomycin, and gramicidin. *Science* **174**, 412–415
49. Boheim, G., Hanke, W., and Eibl, H. (1980) Lipid phase transition in planar bilayer membrane and its effect on carrier- and pore-mediated ion transport. *Proc. Natl Acad. Sci. USA* **77**, 3403–3407
50. Moffat, J.C., Vijayvergiya, V., Gao, P.F., Cross, T.A., Woodbury, D.J., and Busath, D.D. (2008) Proton transport through influenza A virus M2 protein reconstituted in vesicles. *Biophys. J.* **94**, 434–445
51. Brahms, S. and Brahms, J. (1980) Determination of protein secondary structure in solution by vacuum ultraviolet circular dichroism. *J. Mol. Biol.* **138**, 149–178
52. Woody, R.W. (1994) Contributions of tryptophan side chains to the far-ultraviolet circular dichroism of proteins. *Eur. Biophys. J.* **23**, 253–262
53. Salom, D., Hill, B.R., Lear, J.D., and DeGrado, W.F. (2000) pH-dependent tetramerization and amantadine binding of the transmembrane helix of M2 from the influenza A virus. *Biochemistry* **39**, 14160–14170
54. Ladokhin, A.S. (2000) Fluorescence spectroscopy in peptide and protein analysis in *Encyclopedia of Analytical Chemistry* (Meyers, R.A., ed.) pp. 5762–5779, John Wiley and Sons, Chichester
55. McCaul, C.P. and Ludesche, R.D. (1999) Room temperature phosphorescence from tryptophan and halogenated tryptophan analogs in amorphous sucrose. *Photochem. Photobiol.* **70**, 166–171
56. Loewenthal, R., Sancho, J., and Fersht, A.R. (1991) Fluorescence spectrum of barnase: contributions of three tryptophan residues and a histidine-related pH dependence. *Biochemistry* **30**, 6775–6779
57. Mauguen, Y., Hartley, R.W., Dodson, E.J., Dodson, G.G., Bricogne, G., Chothia, C., and Jack, A. (1982) Molecular structure of a new family of ribonucleases. *Nature* **297**, 162–164
58. Dougherty, D.A. (1991) Cation−π interactions in chemistry and biology: a new view of benzene, Phe, Tyr, and Trp. *Science* **271**, 163–168
59. Gallivan, J.P. and Dougherty, D.A. (1999) Cation−π interactions in structural biology. *Proc. Natl Acad. Sci. USA* **96**, 9459–9464
60. Su, C., Wang, Y., and Spiro, T.G. (1990) Saturation effects on ultraviolet resonance Raman intensities: Excimer/YAG laser comparison and aromatic amino acid cross-sections. *J. Raman Spectrosc.* **21**, 435–440
61. Harada, I. and Takeuchi, H. (1986) Raman and ultraviolet resonance Raman spectra of proteins and related compounds in *Spectroscopy of Biological Systems* (Clark, R.J.H. and Hester, R.E., eds.) pp. 113–175, John Wiley and Sons, New York
62. Matsuno, M. and Takeuchi, H. (1998) Effects of hydrogen bonding and hydrophobic interactions on the ultraviolet resonance Raman intensities of indole ring vibrations. *Bull. Chem. Soc. Jpn.* **71**, 851–857
63. Takeuchi, H. (2003) Raman structural markers of tryptophan and histidine side chains in proteins. *Biopolymers* **72**, 305–317

64. Harada, I., Miura, T., and Takeuchi, H. (1986) Origin of the doublet at 1360 and 1340 cm^{-1} in the Raman spectra of tryptophan and related compounds. *Spectrochim. Acta* **42A**, 307–312
65. Miura, T., Takeuchi, H., and Harada, I. (1988) Characterization of individual tryptophan side chains in proteins using Raman spectroscopy and hydrogen-deuterium exchange kinetics. *Biochemistry* **27**, 88–94
66. Xue, Y., Davis, A.V., Balakrishnan, G., Stasser, J.P., Staehlin, B.M., Focia, P., Spiro, T.G., Penner-Hahn, J.E., and O'Halloran, T.V. (2008) Cu(I) recognition via cation-π and methionine interactions in CusF. *Nat. Chem. Biol.* **4**, 107–109